Nano Research

ISSN 1998-0124 CN 11-5974/O4
https://doi.org/10.1007/s12274-024-6537-1

Research Article

Highly adaptive triboelectric tactile sensor on the foot of autonomous wall-climbing robots for detecting the adhesion state and avoiding the hazard

Zhaoyang Wang[1,§], Jianhua Liu[1,§], Ziyu Wang[1,§], Chang Liu[1], Qingyu Chen[2], Chaofan Zhang[2], Wenbo Zhang[3], Jicang Si[1], Xiu Xiao[1] (✉), Peng Xu[1,4] (✉), and Minyi Xu[1] (✉)

[1] *Dalian Key Lab of Marine Micro/Nano Energy and Self-powered System, Marine Engineering College, Dalian Maritime University, Dalian 116026, China*
[2] *Information Science and Technology College, Dalian Maritime University, Dalian 116026, China*
[3] *Navigation College, Dalian Maritime University, Dalian 116026, China*
[4] *Intelligent Biomimetic Design Lab, College of Engineering, Peking University, Beijing 100871, China*
[§] *Zhaoyang Wang, Jianhua Liu, and Ziyu Wang contributed equally to this work.*

Received: 13 December 2023 / **Revised:** 26 January 2024 / **Accepted:** 2 February 2024

ABSTRACT

Due to the excellent maneuverability and obstacle crossing of legged robots, it is possible for an autonomous legged wall-climbing robots to replace manual inspection of ship exterior panels. However, when the magnetic adsorption legged wall-climbing robot steps on the convex point or convex line of the wall, or even when the robot missteps, the robot is likely to detach from the ferromagnetic wall. Therefore, this paper proposes a tactile sensor for the legged magnetic adsorption wall-climbing robot to detect the magnetic adsorption state and improve the safety of the autonomous crawling of the robot. The tactile sensor mainly comprises a three-dimensional (3D)-printed shell, a tactile slider, and three isometric sensing units, with an optimized geometry. The experiment shows that the triboelectric tactile sensor can monitor the sliding depth of the tactile slider and control the light-emitting device (LED) signal light. In addition, in the demonstration experiment of detecting the adsorption state of the robot's foot, the triboelectric tactile sensor has strong adaptability to various ferromagnetic wall surfaces. Finally, this study establishes a robot gait control system to verify the feedback control ability of the triboelectric tactile sensor. The results show that the robot equipped with the triboelectric tactile sensor can recognize the dangerous area on the crawling wall and autonomously avoid the risk. Therefore, the proposed triboelectric tactile sensor has great potential in realizing the tactile sensing ability of robots and enhancing the safety and intelligent inspection of ultra-large vessels.

KEYWORDS

legged wall-climbing robot, ship inspection, tactile perception, triboelectric sensor

1 Introduction

At present, legged wall-climbing robots have emerged as a crucial tool for ship hull inspection due to their high flexibility [1–3]. However, due to the fact that the ship's ferromagnetic metal shell plates typically have complex structures, including various corrosion spots, cracks, and weld seams [4, 5], there is a risk of the robot falling off the wall during the climbing. Thus, ensuring stable adhesion [6, 7] and establishing effective contact between the electromagnets and the wall surface [8, 9] are crucial for the stable movement of the legged wall-climbing robots. To solve this problem, it is urgent to develop a sensor to monitor the magnetic attachment state of the robot's feet during movement [10].

Currently, many researchers have attempted to detect the adhesion state of the legged wall-climbing robots in various ways [10, 11]. For instance, inspired by biological systems, Taewi Kim et al. [12] have developed an ultra-stable and durable crack tactile sensor. The sensor has been integrated into a small legged robot to detect the forces generated by each step of the robot. Additionally, it can determine terrain types, road inclinations, and the static loads applied to the robot. Shukri et al. [13] installed vacuum sensors and photoelectric sensors on the front and rear ends of the robot to ensure stable and reliable adhesion of the wall-climbing robot to the climbing surface. However, vacuum sensors cannot be used for the magnetic adsorption wall-climbing robot, and photoelectric sensors failed to detect the reliability and stability of magnetic adsorption. In order to detect the grasping state of the robot during climbing, Rui Li et al. [14] developed a claw-type foot with a sensing function based on the flexible resistive sensor, which was inspired by domestic cats. Pressure sensors were also commonly used to monitor and detect the suction force states of such robots [15, 16]. However, since the magnetic adsorption force decreases significantly as the distance between the electromagnet and the ferromagnetic metal wall increases, pressure and resistance sensors are unsuitable for mounting on the feet of the magnetic adhesion wall-climbing robots. Tactile sensors are usually mounted on the suction cups of the robot to detect the

Address correspondence to Xiu Xiao, xiaoxiu@dlmu.edu.cn; Peng Xu, pengxu@dlmu.edu.cn; Minyi Xu, xuminyi@dlmu.edu.cn

adhesion state [17, 18]. Compared with other types of sensors, tactile sensors have exhibited superior detection capability in dark and multi-obstacle environments [19–22]. However, there is currently no effective solution available for detecting the adhesion state of the legged wall-climbing robots.

Worth noting, wall-climbing robots that employ magnetic adhesion typically rely on magnetic force to attach to the ferromagnetic surfaces for climbing and fixation [10, 23–26]. Suppose that tactile sensors are placed between the robot's foot and the ferromagnetic surface. In that case, they may cause minor interference or hinder direct contact between the robot's foot and the ferromagnetic wall surface, thereby reducing the stability and reliability of magnetic adhesion. Triboelectric sensors have gained significant attention in recent years due to their ability to convert external stimuli into electrical signals without requiring an external power source [27, 28]. They have been widely used in vibration monitoring [29–31], body motion monitoring [32–35], pressure monitoring [36, 37], speed monitoring [38, 39], environmental monitoring [40, 41] and so on. The triboelectric sensor's operation mechanism includes both triboelectrification and electrostatic induction [42–44]. More importantly, such sensing devices can be designed into different structures to enhance adaptability to various scenarios [45]. Therefore, triboelectric sensors are expected to provide an effective solution for sensing the adhesion state of wall-climbing robots.

In this study, a highly adaptable triboelectric tactile sensor (TTS) was developed for monitoring the adhesion status of the legged magnetic adsorption wall-climbing robots. The triboelectric tactile sensor is embedded into the outer casing of the electromagnet on the robot's foot. When the robot lifts or lands its feet, it will cause contact or separation between the electrode and the dielectric layer, generating an electrical signal. By detecting and converting these signals into control signals for the microcontroller, the robot can assess the reliability of foot adhesion and adjust its gait to avoid hazardous areas.

2 Results and discussion

2.1 Structure and working principle

As depicted in Fig. 1(a)(i), the legged magnetic adsorption wall-climbing robot performs inspection tasks of the hull plate. The robot may step on linearly raised welding seams, misstep, or convex points (such as point-like corrosion) (Figs. 1(a)(ii)–1(a)(iv)). When these abnormal wall conditions are encountered, the robot is highly prone to the risk of falling off the ferromagnetic wall surface. The triboelectric tactile sensor is designed to be mounted on the foot of the robot. When the robot crawls on the surface of the hull plate, the triboelectric tactile sensor can generate electrical signals to detect the magnetic

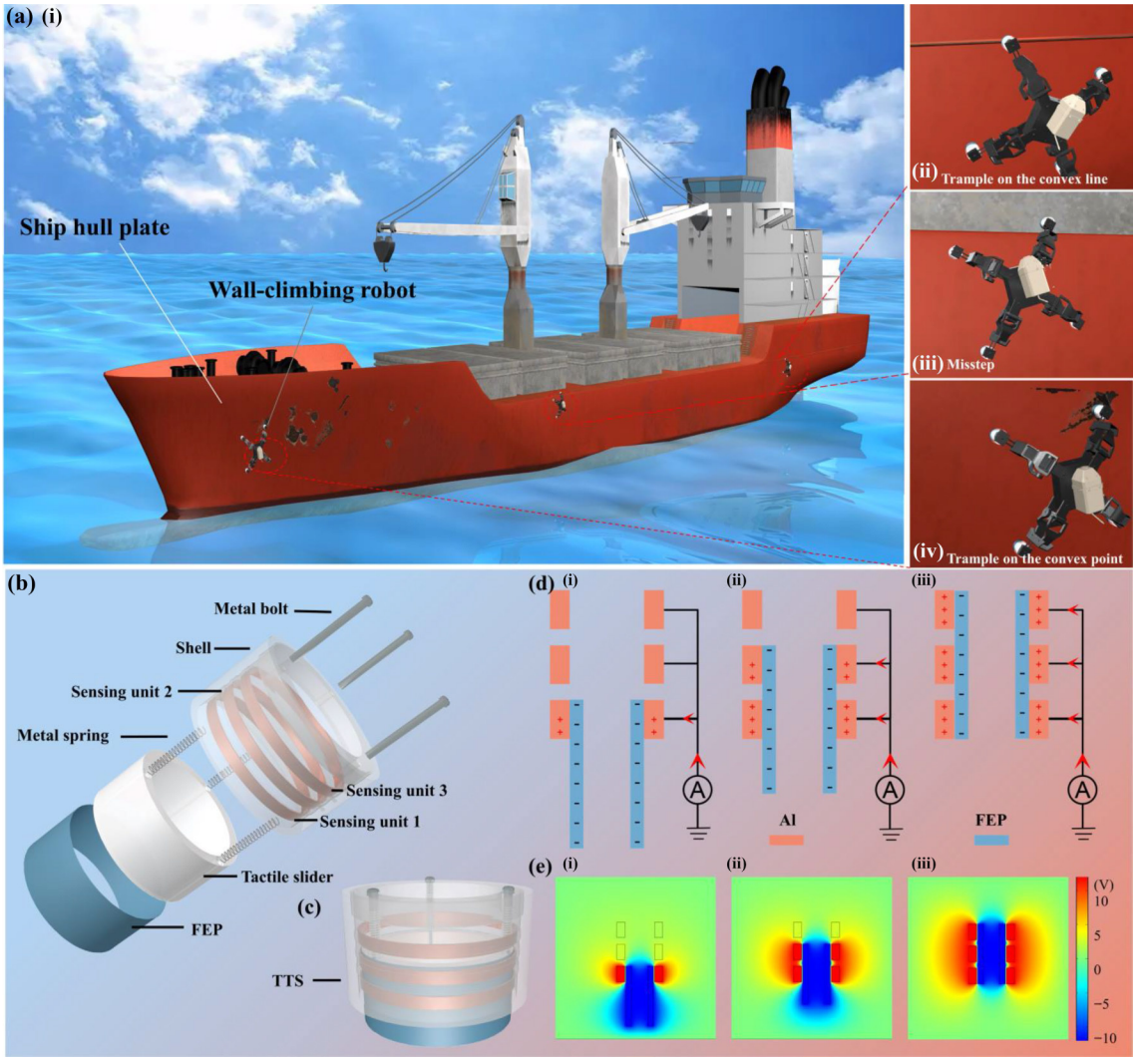

Figure 1 Structure, principle and application of the triboelectric tactile sensor. (a)(i) The legged magnetic adsorption wall-climbing robot installed with TTS. (a)(ii)–(a)(iv) The triboelectric tactile sensor installed on the legged magnetic adsorption wall-climbing robot detects the convex line, misstep, and convex point. (b) The structure and components of the triboelectric tactile sensor. (c) Image of an triboelectric tactile sensor. (d) The charge transfer process of the triboelectric tactile sensor when the robot's foot tramples on the ground. (e) The simulation of potential distribution using COMSOL software.

attachment of the foot. More importantly, when the robot steps on convex points or missteps, the triboelectric tactile sensor will generate abnormal signals reflecting the real-time magnetic adsorption status, improving the robot's safety. The specific signal analysis can be found in Sections B and C.

Figure 1(b) illustrates the detailed structural components of TTS. As shown in Fig.S1 in the Electronic Supplementary Material (ESM), it is composed of five parts, including a three-dimensional (3D)-printed shell, three sensing units made of aluminum electrodes, a tactile slider enveloped in fluorinated ethylene propylene (FEP) film, three metal bolts to position the tactile slider, and three metal springs used to restore the initial position of the tactile slider. The shell of the sensor is made of photosensitive resin and is fixed on the exterior of the electromagnet to provide support for other components. The photosensitive resin offers high manufacturing precision and wear resistance, making it ideal for supporting the 3D-printed tactile slider. The three sensing units are arranged equidistant inside the shell and are labeled as sensing unit 1 (S1), sensing unit 2 (S2), and sensing unit 3 (S3) from bottom to top, respectively. The three metal bolts with a diameter of 2.5 mm inside the shell provide guidance and support for the tactile slider, and the three metal springs with a length of 2.0 cm are fixed to the sensor housing at one end and the tactile slider at the other end. The movement of the tactile slider causes the FEP film to rub against the three sensing units, resulting in charge transfer with different characteristics. Figure 1(c) provides an integrated diagram of the triboelectric tactile sensor device.

The working mechanism of the triboelectric sensor is shown in Fig. 1(d). When the robot installed with TTS steps onto the wall, the tactile slider is subjected to upward pressure and slides along the metal bolt toward the interior of the triboelectric tactile sensor shell. As a result, the aluminum electrode on the sensing unit comes into contact with the FEP film on the tactile slider. Fig. 1(d)(i) demonstrates the initial contact of the tactile slider with the aluminum electrode on S1 of the triboelectric tactile sensor. As a result, the positive charge on the aluminum electrode increases due to the triboelectric and electrostatic effects, and the current signal flows from the aluminum electrode to the ground. Subsequently, the FEP film on the tactile slider makes contact with S2 and S3 in turn, generating positive current signals in the external circuit, as shown in Figs. 1(d)(ii) and 1(d)(iii). When the robot lifts its foot, the tactile slider moves outwards along the shell under the elastic force exerted by the metal spring, and the working mechanism of the triboelectric sensor is depicted in Fig. S3 in the ESM. This displacement reduces the accumulated positive charges on the aluminum electrode, causing electrons to flow from the ground towards the aluminum electrode and generating a reverse current signal within the external circuit. Furthermore, the COMSOL Multiphysics software was utilized to simulate the potential distribution between the FEP and aluminum electrodes. The simulation results in Fig. 1(e) are consistent with the above principle analysis.

2.2 Output performance of the triboelectric tactile sensor

A tactile sensor signal test platform was built to study the electrical output performance of the triboelectric tactile sensor, as shown in Fig. 2(a). Since all sensing units work on the same principle, only sensing unit 3 was used as a demonstration in the following experiment (see the Experiment Section in the ESM for details).

The influence of dielectric material on the electrical output of TTS is firstly studied and the results are depicted in Fig.2(b). Five different materials, which were polyethylene terephthalate (PET), polytetrafluoroethylene (PTFE), Kapton, FEP, and polyvinyl chloride (PVC), were tested. The triboelectric tactile sensor demonstrated a peak open-circuit voltage (V_{oc}) of 12.3 V when FEP was utilized as the triboelectric layer material. A higher electrical output signifies a higher sensitivity of the sensor. Therefore, the FEP film was chosen as the triboelectric layer for TTS. The width of the aluminum electrode is the other crucial factor affecting the electrical output performance of TTS. As displayed in Figs. 2(c) and 2(d), the V_{oc} and short-circuit current (I_{sc}) of the sensing unit increased from 7.28 to 11.66 V and from 12.64 to 22.29 nA, respectively, as the width of the aluminum electrode increased from 1.0 to 3.0 mm. The relationship between the I_{sc} and the width of the electrode was established using the leave-one-out cross-validation strategy, as shown in Fig. 2(e). The model showed a strong linear correlation with a coefficient of determination (R^2) of 0.99347 and a maximum error of 0.49% at the width of 1.5 mm. In order to achieve the optimal output performance of TTS, the aluminum electrode with a width of 3.0 mm was adopted.

Moreover, the impact of motor frequency on the electrical output of TTS was investigated to validate its sensitivity to the pedaling frequency of the robot. As shown in Fig. 2(f), the V_{oc} of TTS remained around 12 V as the motor frequency increased from 0.2 to 2.0 Hz. This indicated that the sensing capability of the triboelectric tactile sensor is not affected by frequency. In addition, Fig. 2(g) shows the variation of output voltage with the motor frequency at different electrode widths. For each electrode width, the output voltage basically didn't change with frequency, and the maximum deviation was 1.16%. However, the I_{sc} of TTS increased from 1.17 to 20 nA as the frequency raised from 0.2 to 2.0 Hz, as shown in Fig. 2(h). This is caused by the fact that a higher frequency denotes a larger amount of contact-separation and transferred charge per unit time. Similarly, a leave-one-out cross-validation strategy was used to establish the relationship between the I_{sc} and the motor frequency, as shown in Fig. 2(i). A strong linear relationship was found with a correlation coefficient of 0.98014 and a maximum error of −1.35%. Therefore, the output current signal can be used to characterize the working frequency of TTS with high precision.

It is worth noting that the working environment of robots is usually harsh and changeable, so it is necessary to conduct sensitivity tests of the triboelectric tactile sensor to ambient temperature and humidity. The electrical output performance of TTS was measured in an experimental platform where the temperature could be adjusted, as depicted in Fig. S4 in the ESM. Figure 2(j) illustrates that the V_{oc} of TTS remained constant at about 12 V as the temperature increased from 20 to 40 °C. This result indicates that the sensing unit of the triboelectric tactile sensor can work normally in environments with varying temperature levels. Subsequently, a series of experiments were carried out under different relative humidity conditions. Figure 2(k) reveals that the V_{oc} of TTS exhibits constancy, hovering around 12 V, even with an increase in relative humidity from 50% to 90%. This observation suggests that the triboelectric tactile sensor is capable of upholding stable performance despite significant changes in humidity levels. Furthermore, a durability test was conducted on the triboelectric tactile sensor. As can be seen in Fig. 2(l), the sensing unit of TTS demonstrated a consistent output voltage of approximately 12 V even after one month. Figure S5 in the ESM further demonstrates the detailed output performance of TTS to confirm its long-term durability. Therefore, the as-proposed triboelectric tactile sensor not only performs effectively under different temperature and humidity conditions, but also exhibits excellent durability, making it suitable for various application scenarios that require reliable and robust tactile sensing.

As a matter of fact, the robot often needs to work on hull plates with certain inclination angles. In this part, sensor performance

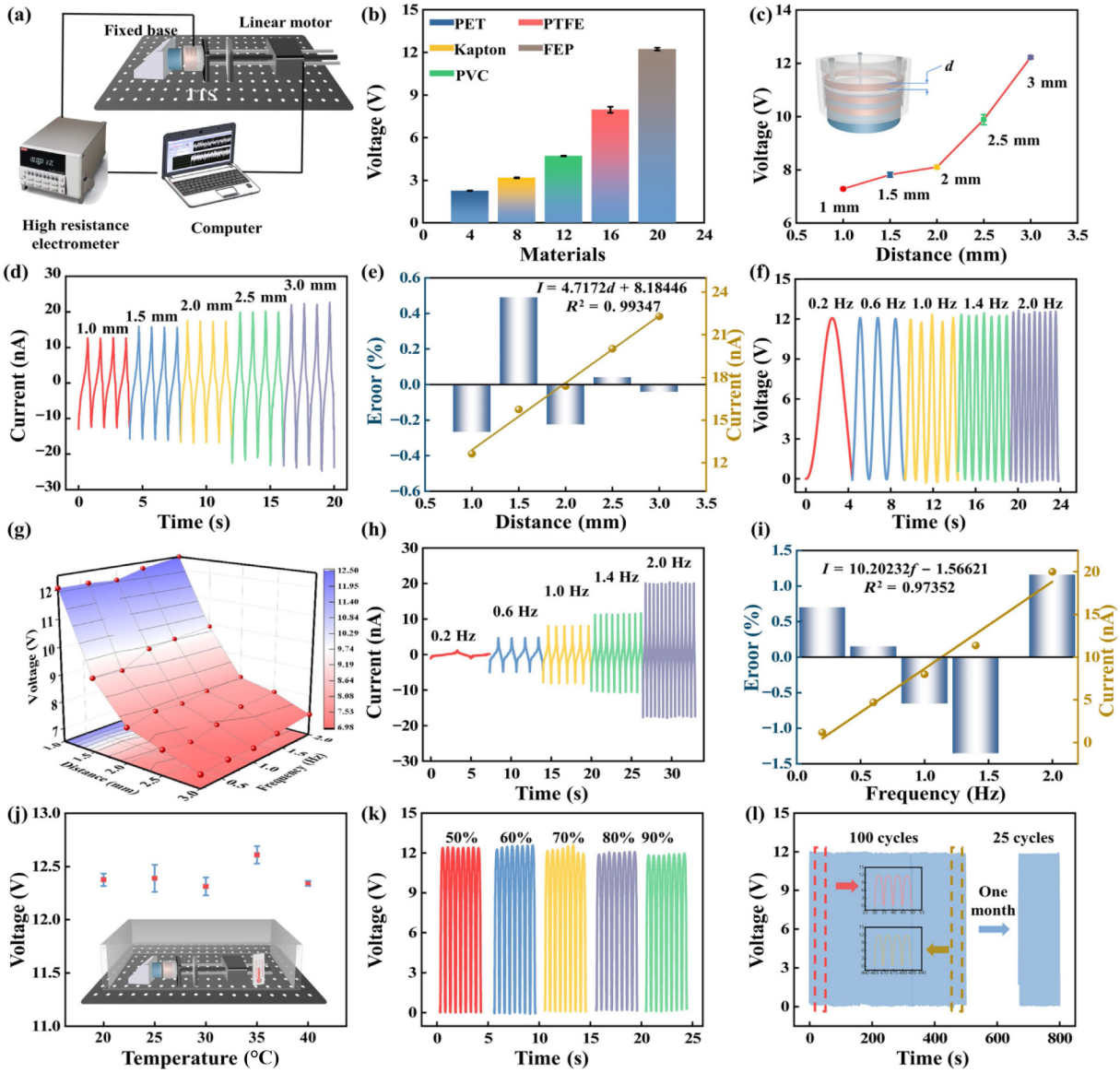

Figure 2 Output performance of the triboelectric tactile sensor. (a) Schematic diagram of the experimental setup. (b) Influence of dielectric material (FEP, PTFE, PET, Kaptopn, and PVC) on the electrical output of TTS. Influence of electrode width on (c) V_{oc} and (d) I_{sc}. (e) A fitting linear relationship between V_{oc} and electrode width. Influence of external frequency on (f) V_{oc} and (h) I_{sc}. (g) Influence of external load frequency and width of the aluminum electrode on V_{oc}. (i) A fitting linear relationship between I_{sc} and external load frequency. (j) Influence of ambient temperature on V_{oc}. (k) Influence of relative humidity on V_{oc}. (l) Durability test diagram of the triboelectric tactile sensor.

tests were conducted with wall inclination ranging from 15° to 60°. Figure 3(a) illustrates the V_{oc} of sensing unit 3 under various wall slopes. It can be observed that as the inclination angle of the wall increases, the V_{oc} remains stable at round 12 V. The output of the other two sensing units is consistent with this result, as shown in Fig. 3(b). These findings indicate that the triboelectric tactile sensor has reliable output at different slope angles, which is crucial for the sensing performance of the robot.

Significantly, the electrical output of TTS can reflect the insertion depth of the slider, thereby revealing the magnetic adsorption state of the robot's foot. As shown in Fig. S6 in the ESM, a visualization interface that allows the real-time display of the insertion depth based on the V_{oc} of the triboelectric sensor was developed using LabVIEW. The logic diagram for tactile monitoring is depicted in Fig. 3(c). The different insertion depths of the tactile slider were achieved by adjusting the stroke of the linear motor, as illustrated in Fig. S7 in the ESM. The high resistance electrometer receives electrical signals from TTS, and the data is then processed through low-pass filtering and transferred to LabVIEW. The visualization interface image displays the V_{oc} of TTS and the corresponding insertion depths in real time. It can be seen from Movie ESM1 that the triboelectric tactile sensor exhibits excellent sensing capability. This LabVIEW-based visualization interface enhances the understanding and analysis of the adsorption status of the robot's foot by providing real-time visual feedback. It enables researchers and users to monitor and analyze the behavior of the robot accurately.

Since the three sensing units generate signals independently, this provides an intuitive scheme for tactile sensor signal monitoring, that is, using the electrical output of each sensing unit to control different light-emitting devices (LEDs). The circuit diagram in Fig. S8 in the ESM illustrates the scheme of using triboelectric tactile sensor to illuminate LED and the experimental setup is presented in Fig. S9 in the ESM. An Arduino-Uno board was employed to receive signals and process data. Notably, each sensing unit controls a different LED, and the quantity of the illuminated LEDs corresponds to the number of the sensing units as well as the insertion depth. Figure 3(d) demonstrates that as the tactile slider of the triboelectric tactile sensor is compressed to different positions, the three sensing units sequentially generate

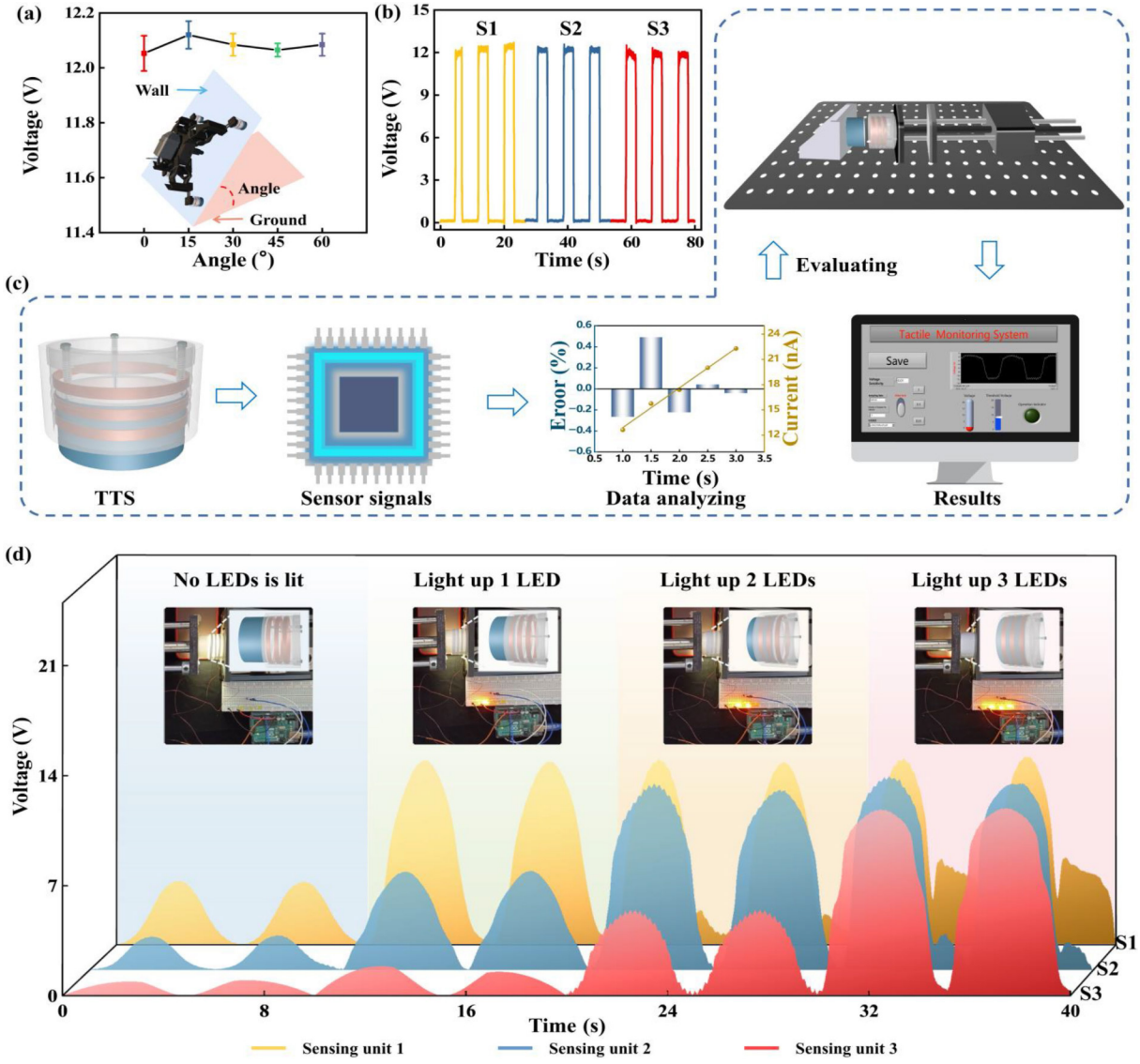

Figure 3 Application of the triboelectric tactile sensor in external load monitoring. (a) Influence of inclination angle on V_{oc} of S3. (b) Output voltage V_{oc} of the triboelectric tactile sensor. (c) A logical block diagram is used to monitor the insertion depth of the tactile slider. (d) The output signals of the triboelectric tactile sensor for controlling LEDs.

electrical signals and light up the corresponding LED. In Movie ESM2, it can be observed that when the tactile slider of the triboelectric tactile sensor is compressed to the position of sensing unit 1, the first LED is illuminated. This occurs because the output voltage of the respective sensing unit reaches the preset trigger value of 12 V for activating the LED. Furthermore, when the slider is compressed to the positions of sensing units 2 and 3, the second and third LEDs are illuminated respectively. The triboelectric tactile sensor demonstrates its effective sensing capability by detecting voltage signals outputted from the sensing units.

2.3 Demonstration of the triboelectric tactile sensor

The system architecture diagram of the robot is illustrated in Fig. 4(a). Since the control and action principles of the robot's four legs are basically the same, only one leg is exhibited in the logic diagram (see the system architecture diagram of the robot section in the ESM for details). The three-channel signals from TTS are acquired in real time using an Arduino-Uno board. These acquired signals are then transmitted via serial communication and displayed in real time on the LABVIEW interface. The slope angle of the ferromagnetic wall is set at 15° to simulate the real scenario.

As shown in Fig. 4(b), the area beyond the edge of the steel plate is used for the misstep simulation of the robot. Figure 4(c) displays the voltage signals obtained from the triboelectric tactile sensor when the robot missteps. During normal walking, when the leg equipped with TTS is lifted, the three sensing units of the triboelectric tactile sensor generate real-time voltage signals. Specifically, S3 is firstly detached from the tactile slider to generate a voltage drop signal, and then S2 and S1 sequentially produce similar voltage drop signals. When the robot's foot re-steps on the steel plate, sensing unit 1 first rubs against the tactile slider to generate an increased voltage signal, and then followed by S2 and S3. However, when the robot missteps, the tactile slider cannot rub against the sensing units. As a result, the three sensing units of TTS do not generate any increased voltage signals after the foot lands.

Furthermore, a curved raised obstacle with a height of 1.0 cm is used to simulate the metal weld on the ship's hull, as shown in Fig. 4(d), and the sensing results are demonstrated in Fig. 4(e). When the foot of the robot steps on a simulated welded joint of the steel plate, only S1 rubs against the tactile slider since the triboelectric tactile sensor is not fully compressed, resulting in no increased voltage signals from S2 and S3. Finally, as displayed in Fig. 4(f), a pitting-shaped convexity is employed to simulate the corrosion point of the ferromagnetic metal wall, and the output of TTS can

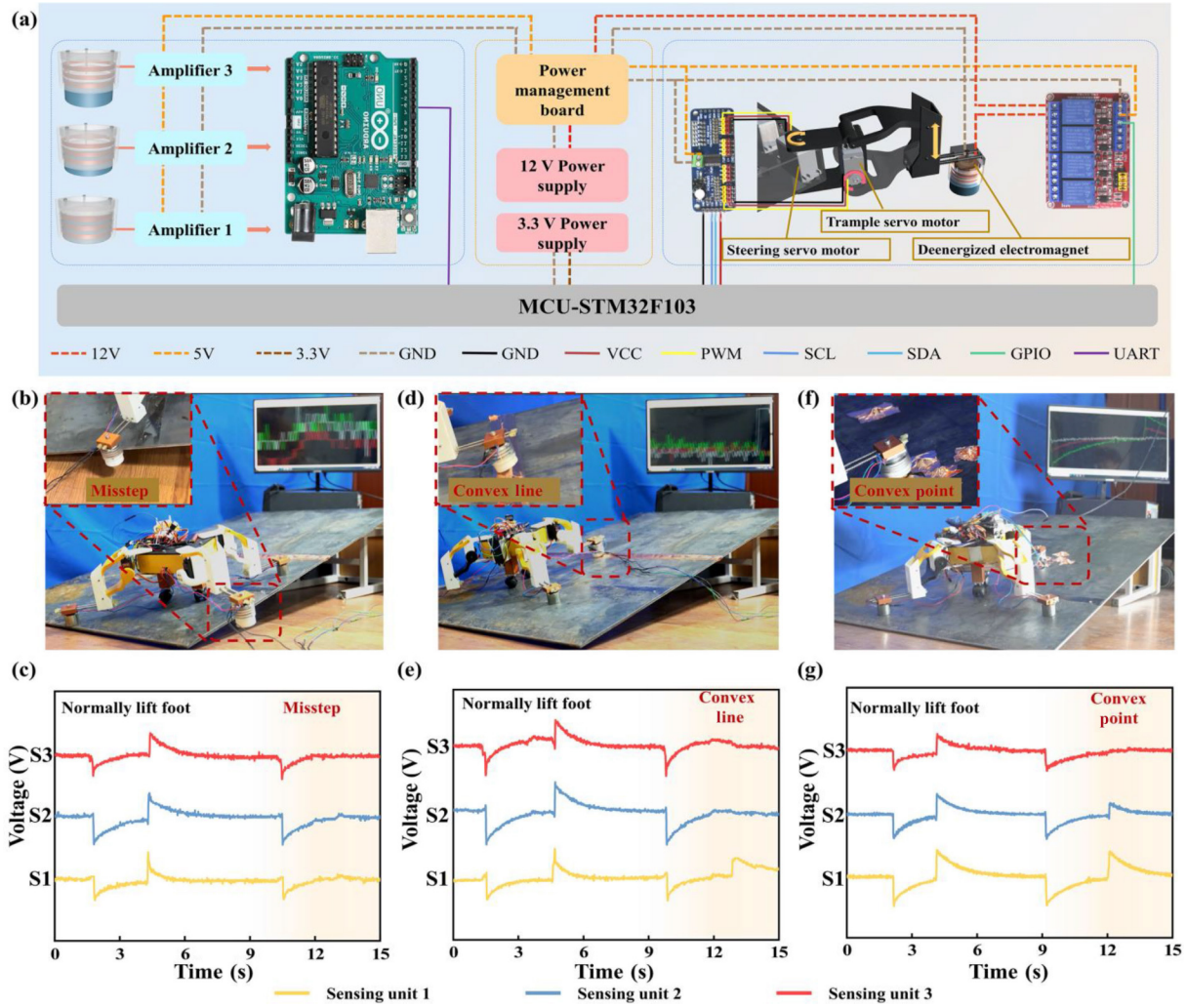

Figure 4 Experiment of TTS detecting the foot adsorption status. (a) System schematic of the triboelectric tactile sensor for the legged magnetic adsorption wall-climbing robot. (b), (d) and (f) Sensor configuration and experimental scene layout under different wall surfaces. (c), (e) and (g) The output signals of the triboelectric tactile sensor for detecting foot adsorption status under different wall conditions.

be found in Fig. 4(g). When the robot steps on a simulated corrosion point, the triboelectric tactile sensor cannot be fully compressed due to the uneven wall surface, and the tactile slider can only rub against S1 and S2. Hence, no increased voltage signal is generated from S3. These demonstrations confirm that TTS can detect whether the robot's foot is tightly compressed due to the uneven wall surface, and the tactile slider can only rub against S1 and S2. Hence, no increased voltage signal is generated from S3. These demonstrations confirm that TTS can detect whether the robot's foot is tightly attached to the ferromagnetic wall surface, thus providing support for the feedback control of the robot using the triboelectric tactile sensor.

Figure 5(a) illustrates the control algorithm logic for acquiring the triboelectric tactile sensor signal using Arduino-Uno and processing the feedback to the microcontroller unit (MCU). In specific, prior to stepping onto the ground during the normal walking of the robot, the robot's MCU sends a signal to Arduino-Uno via the serial port to instruct it to detect and record the signals from the three sensing units at that time. These signals are denoted as U_1, U_2 and U_3, respectively. The robot can proceed with its stepping motion if Arduino-Uno successfully collects these signals from TTS. Once the robot steps onto the ground, the MCU immediately sends a signal to Arduino-Uno through the serial port to acquire and record the voltage signals from the sensing units S1, S2, and S3. These recorded signals are then labeled as U_1', U_2' and U_3', respectively. If no voltage signal is acquired from these sensing units, it indicates an abnormal operating status of the robot. In this case, the robot is stopped urgently. If the voltage signals are successfully acquired, the next step of calculating the difference between the two voltage signals of each channel, which are denoted as $\Delta U_1 = U_1' - U_1$, $\Delta U_2 = U_2' - U_2$ and $\Delta U_3 = U_3' - U_3$, is proceeded. If ΔU_1 is not greater than 3 V, it indicates that the robot's foot has completely misstepped, and it is very dangerous for the robot to continue walking. Therefore, by communicating with the serial port of the MCU, the robot is directed to enter the steering motion until its foot adheres to the ferromagnetic wall and resumes walking forwards. The motion gaits of forward walking and steering are shown in Figs. 5(b) and 5(c), respectively. On the other hand, if ΔU_1, ΔU_2, and ΔU_3 are greater than 3 V, it indicates that the foot is firmly attached to the wall. In this case, the robot can either continue to walk forward or transit from steering motion to forward walking (see Movie ESM3).

As depicted in Fig. 5(d), the robot with TTS mounted on its foot is climbing on a ferromagnetic wall with a slope of 15°. Under normal walking conditions, the triboelectric tactile sensor continuously generates voltage signals. However, if the robot's foot happens to misstep abruptly, none of the three channels of TTS generate any voltage signals. Because we set the TTS detection algorithm to be implemented only after the robot's stampede action occurs. In response, the MCU controls the robot to perform a steering motion. After successfully adjusting its position, the robot steps onto the steel plate again to avoid the risk of falling due to misstep, as demonstrated in the Movie ESM3.

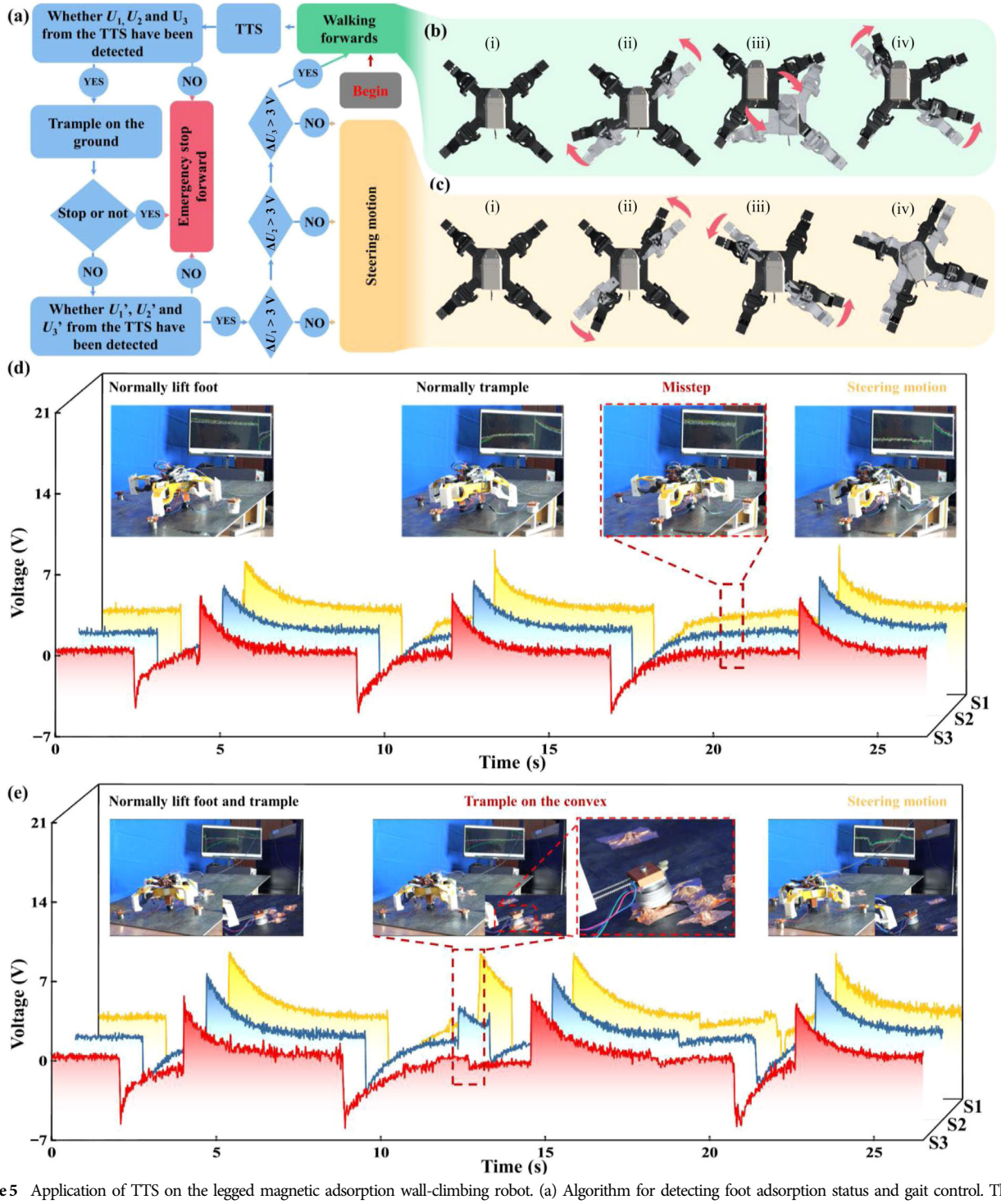

Figure 5 Application of TTS on the legged magnetic adsorption wall-climbing robot. (a) Algorithm for detecting foot adsorption status and gait control. The (b) straight walking gait and (c) steering gait of the legged magnetic adsorption wall-climbing robot. The output signals of TTS for detecting foot adsorption status when the robot (d) missteps and (e) tramples on the convex point.

When the robot's foot comes into contact with the convex on the wall surface, as shown in Fig. 5(e), the third sensing unit of the triboelectric tactile sensor fails to generate a voltage signal. Consequently, the MCU commands the robot to execute a steering motion and resume walking with a straight-line gait, which effectively avoids the potential danger of falling (see Movie ESM4).

3 Conclusion

In this study, a triboelectric tactile sensor was developed for detecting the adhesion state of the legged wall-climbing robot's foot and gait control. The triboelectric tactile sensor consists of three equidistant sensing units and works based on the contact-separation between the aluminum electrodes and the FEP film coated on the tactile slider. The effects of dielectric material, the width of the electrode, the stepping frequency, and the wall inclination angle have been investigated to optimize and verify the electrical output performance of TTS. The application of TTS for monitoring the sliding depth of the tactile slider and controlling LED signal lights confirmed its effectiveness in monitoring the magnetic adsorption state of the robot's foot on the ferromagnetic wall. This validation further supports the feasibility of using the triboelectric tactile sensor as a foot tactile sensor.

Furthermore, a set of gait control systems were established to demonstrate the feedback control capability of the robot with TTS

installed on its foot. Results indicate that the robot equipped with the triboelectric tactile sensor can recognize the dangerous area on the crawling wall and autonomously avoid the risk, including convex points or lines and missteps. Therefore, the as-proposed triboelectric tactile sensor holds great potential for enabling tactile sensing of the legged robots and enhancing the safety and intelligent inspection of large vessels.

Acknowledgements

This work was supported by the Dalian Outstanding Young Scientific and Technological Talents Project (No. 2021RJ11), and the Science and Technology Innovation Foundation of Dalian (No. 2021JJ12GX028).

Electronic Supplementary Material: Supplementary material (system architecture diagram of the robot section, demonstration of tactile monitoring system, application of TTS to control LEDs, application of TTS to control the robot to avoid misstep, application of TTS to control the robot to avoid convex point) is available in the online version of this article at https://doi.org/10.1007/s12274-024-6537-1.

References

[1] Vlasova, N. S.; Bykov, N. V. The problem of adhesion methods and locomotion mechanism development for wall-climbing robots. 2019, arXiv: 1905.09214. arXiv.org e-Print archive. https://arxiv.org/abs/1905.09214 (accessed May 22, 2019).

[2] Hajeer, A.; Chen, L.; Hu, E. Review of classification for wall climbing robots for industrial inspection applications. In *Proceedings of the 2020 IEEE 16th International Conference on Automation Science and Engineering*, Hong Kong, China, 2020, pp 1421–1426.

[3] Fang, Y.; Wang, S.; Bi, Q. S.; Cui, D.; Yan, C. L. Design and technical development of wall-climbing robots: A review. *J. Bionic Eng.* **2022**, *19*, 877–901.

[4] Huang, H. C.; Li, D. H.; Xue, Z.; Chen, X. L.; Liu, S. Y.; Leng, J. X.; Wei, Y. Design and performance analysis of a tracked wall-climbing robot for ship inspection in shipbuilding. *Ocean Eng.* **2017**, *131*, 224–230.

[5] Wang, B.; Ni, Z. F.; Shen, Y.; Zhang, S.; Shen, Q.; Niu, X. W. Design and analysis of a wheel-leg compound variable curvature ship hull cleaning robot. *Ocean Eng.* **2022**, *266*, 112755.

[6] Silva, M. F.; Machado, J. A. T.; Tar, J. K. A survey of technologies for climbing robots adhesion to surfaces. In *Proceedings of 2008 IEEE International Conference on Computational Cybernetics*, Stara Lesna, Slovakia, 2008, pp 127–132.

[7] Kapula, P. R.; Ram, M. B.; Chakradhar, M. S.; Shravani, K.; Akhilesh, K.; Likhitha, K. L. Design of an adhesion-based wall climbing robot. In *Proceedings of the 2023 2nd International Conference on Vision Towards Emerging Trends in Communication and Networking Technologies*, Vellore, India, 2023, pp 1–6.

[8] Hu, J. Y.; Han, X.; Tao, Y. R.; Feng, S. Z. A magnetic crawler wall-climbing robot with capacity of high payload on the convex surface. *Robot. Auton. Syst.* **2022**, *148*, 103907.

[9] Zhu, L. S.; Zheng, X. S. Design of a curved surface adaptive permanent magnet wall climbing robot. *J. Phys. Conf. Ser.* **2022**, *2405*, 012028.

[10] Hong, S.; Um, Y.; Park, J.; Park, H. W. Agile and versatile climbing on ferromagnetic surfaces with a quadrupedal robot. *Sci. Robot.* **2022**, *7*, eadd1017.

[11] Zhu, H. F.; Guan, Y. S.; Wu, W. Q.; Zhang, L. M.; Zhou, X. F.; Zhang, H. Autonomous pose detection and alignment of suction modules of a biped wall-climbing robot. *IEEE/ASME Trans. Mechatron.* **2015**, *20*, 653–662.

[12] Kim, T.; Hong, I.; Kim, M.; Im, S.; Roh, Y.; Kim, C.; Lim, J.; Kim, D.; Park, J.; Lee, S. et al. Ultra-stable and tough bioinspired crack-based tactile sensor for small legged robots. *npj Flex. Electron.* **2023**, *7*, 22.

[13] Zainal Abidin, M. S.; Amin, S. H. M. On the development a pneumatic four-legged mechanism autonomous vertical wall climbing robot. In *Proceedings of 1998 Malaysian Science and Techology Congress*, Pulan Pinang, Malaysia, 1999.

[14] Li, R.; Yan, S.; Zhou, C. C.; Liu, Z. B.; Shou, M. J. Design of the paw of wall-climbing robot with spiny and sensing function. *J. Phys. Conf. Ser.* **2023**, *2537*, 12009.

[15] Aslam, D. M.; Dangi, G. D. Design, fabrication and testing of a smart robotic foot. *Robot. Auton. Syst.* **2005**, *51*, 207–214.

[16] Zhang, H. X.; Zhang, J. W.; Zong, G. H.; Wang, W.; Liu, R. Sky cleaner 3: A real pneumatic climbing robot for glass-wall cleaning. *IEEE Robot. Autom. Mag.* **2006**, *13*, 32–41.

[17] Hu, B. S.; Xue, J. T.; Jiang, D. J.; Tan, P. C.; Wang, Y. Q.; Liu, M. H.; Yu, H. L.; Zou, Y.; Li, Z. Wearable exoskeleton system for energy harvesting and angle sensing based on a piezoelectric cantilever generator array. *ACS Appl. Mater. Interfaces* **2022**, *14*, 36622–36632.

[18] Zou, Y.; Gai, Y. S.; Tan, P. C.; Jiang, D. J.; Qu, X. C.; Xue, J. T.; Ouyang, H.; Shi, B. J.; Li, L. L.; Luo, D. et al. Stretchable graded multichannel self-powered respiratory sensor inspired by shark gill. *Fundam. Res.* **2022**, *18*, 619–628.

[19] Liu, J. H.; Xu, P.; Zheng, J. X.; Liu, X. Y.; Wang, X. Y.; Wang, S. Y.; Guan, T. Z.; Xie, G. M.; Xu, M. Y. Whisker-inspired and self-powered triboelectric sensor for underwater obstacle detection and collision avoidance. *Nano Energy* **2022**, *101*, 107633.

[20] Xu, P.; Liu, J. H.; Liu, X. Y.; Wang, X. Y.; Zheng, J. X.; Wang, S. Y.; Chen, T. Y.; Wang, H.; Wang, C.; Fu, X. P. et al. A bio-inspired and self-powered triboelectric tactile sensor for underwater vehicle perception. *npj Flex. Electron.* **2022**, *6*, 25.

[21] Xu, P.; Wang, X. Y.; Wang, S. Y.; Chen, T. Y.; Liu, J. H.; Zheng, J. X.; Li, W. X.; Xu, M. Y.; Tao, J.; Xie, G. M. A triboelectric-based artificial whisker for reactive obstacle avoidance and local mapping. *Research* **2021**, *2021*, 9864967.

[22] Song, Z. W.; Yin, J. H.; Wang, Z. H.; Lu, C. Y.; Yang, Z.; Zhao, Z. H.; Lin, Z. N.; Wang, J. Y.; Wu, C. S.; Cheng, J. et al. A flexible triboelectric tactile sensor for simultaneous material and texture recognition. *Nano Energy* **2022**, *93*, 106798

[23] Jose, J.; Dinakaran, D.; Ramya, M. M.; Harris Samuel, D. G. A survey on magnetic wall-climbing robots for inspection. *Int. J. Mech. Prod. Eng. Res. Dev.* **2018**, *8*, 59–68.

[24] Wang, S. Y. Research status and future development of wall-climbing robot. In *Proceedings of 2021 International Conference on Electronics, Circuits and Information Engineering*, Zhengzhou, China, 2021, pp 122–130.

[25] Chen, X. L.; Wu, Y. P.; Hao, H. D.; Shi, H. L.; Huang, H. C. Tracked wall-climbing robot for calibration of large vertical metal tanks. *Appl. Sci.* **2019**, *9*, 2671.

[26] Xu, Z. L.; Ma, P. S. A wall-climbing robot for labelling scale of oil tank's volume. *Robotica* **2002**, *20*, 209–212.

[27] Meng, H. Y.; Yu, Q.; Liu, Z.; Gai, Y. S.; Xue, J. T.; Bai, Y.; Qu, X. C.; Tan, P. C.; Luo, D.; Huang, W. W. et al. Triboelectric performances of biodegradable polymers. *Matter* **2023**, *6*, 4274–4290.

[28] Li, Y. H.; Yu, J. R.; Wei, Y. C.; Wang, Y. F.; Feng, Z. Y.; Cheng, L. Q.; Huo, Z. W.; Lei, Y. Q.; Sun, Q. J. Recent progress in self-powered wireless sensors and systems based on TENG. *Sensors* **2023**, *23*, 1329.

[29] Liu, J. R.; Huang, H.; Zhou, Q.; Wu, C. Self-powered downhole drilling tools vibration sensor based on triboelectric nanogenerator. *IEEE Sens. J.* **2022**, *22*, 2250–2258.

[30] Zhu, J.; Hou, X. J.; Niu, X. S.; Guo, X. P.; Zhang, J.; He, J.; Guo, T.; Chou, X. J.; Xue, C. Y.; Zhang, W. D. The d-arched piezoelectric-triboelectric hybrid nanogenerator as a self-powered vibration sensor. *Sens. Actuators A Phys.* **2017**, *263*, 317–325.

[31] Zhao, H. F.; Shu, M. R.; Ai, Z. H.; Lou, Z. R.; Sou, K. W.; Lu, C. Y.; Jin, Y. C.; Wang, Z. H.; Wang, J. Y.; Wu, C. S. et al. A highly sensitive triboelectric vibration sensor for machinery condition monitoring. *Adv. Energy Mater.* **2022**, *12*, 2201132.

[32] Li, P.; Liu, Y. B.; Zhang, H.; Hu, Z. P.; Jia, L. N.; Liu, D. K.; Yu, L.; Li, B.; Yao, Y. W. All-nanofiber self-powered PTFE/PA66 device

for real-time breathing monitor by scalable solution blow spinning technology. *Nano Res.* **2022**, *15*, 8458–8464.

[33] Xu, J. H.; Wei, X. L.; Li, R. N.; Shi, Y. P.; Peng, Y. T.; Wu, Z. Y.; Wang, Z. L. Intelligent self-powered sensor based on triboelectric nanogenerator for take-off status monitoring in the sport of triple-jumping. *Nano Res.* **2022**, *15*, 6483–6489.

[34] Das, P. S.; Chhetry, A.; Maharjan, P.; Rasel, M. S.; Park, J. Y. A laser ablated graphene-based flexible self-powered pressure sensor for human gestures and finger pulse monitoring. *Nano Res.* **2019**, *12*, 1789–1795.

[35] Tan, P. C.; Han, X.; Zou, Y.; Qu, X. C.; Xue, J. T.; Li, T.; Wang, Y. Q.; Luo, R. Z.; Cui, X.; Xi, Y. et al. Self-powered gesture recognition wristband enabled by machine learning for full keyboard and multicommand input. *Adv. Mater.* **2022**, *34*, 2200793.

[36] Yang, Q. Y.; Yang, S. Q.; Qiu, P. F.; Peng, L. M.; Wei, T. R.; Zhang, Z.; Shi, X.; Chen, L. D. Flexible thermoelectrics based on ductile semiconductors. *Science* **2022**, *377*, 854–858.

[37] Liu, J. H.; Xu, P.; Liu, B.; Xi, Z. Y.; Li, Y. Z.; Guo, L. N.; Guan, T. Z.; Zhu, P.; Meng, Z. C.; Wang, S. Y. et al. Underwater biomimetic lateral line sensor based on triboelectric nanogenerator for dynamic pressure monitoring and trajectory perception. *Small*, in press, DOI: 10.1002/smll.202308491.

[38] Wang, Y.; Wu, C.; Yang, S. A self-powered rotating speed sensor for downhole motor based on triboelectric nanogenerator. *IEEE Sens. J.* **2021**, *21*, 4310–4316.

[39] Zhang, X. S.; Gao, Q.; Gao, Q.; Yu, X.; Cheng, T. H.; Wang, Z. L. Triboelectric rotary motion sensor for industrial-grade speed and angle monitoring. *Sensors* **2021**, *21*, 1713.

[40] Qin, Y. H.; Fu, X. P.; Lin, Y.; Wang, Z.; Cao, J.; Zhang, C. Self-powered internet of things sensing node based on triboelectric nanogenerator for sustainable environmental monitoring. *Nano Res.* **2023**, *16*, 11878–11884.

[41] Zhang, B. S.; Li, W. B.; Ge, J. W.; Chen, C. G.; Yu, X.; Wang, Z. L.; Cheng, T. H. Single-material-substrated triboelectric-electromagnetic hybrid generator for self-powered multifunctional sensing in intelligent greenhouse. *Nano Res.* **2023**, *16*, 3149–3155.

[42] Cheng, T. H.; Shao, J. J.; Wang, Z. L. Triboelectric nanogenerators. *Nat. Rev. Methods Primers* **2023**, *3*, 39.

[43] Zhou, Y. K.; Shen, M. L.; Cui, X.; Shao, Y. C.; Li, L. J.; Zhang, Y. Triboelectric nanogenerator based self-powered sensor for artificial intelligence. *Nano Energy* **2021**, *84*, 105887.

[44] Kim, W. G.; Kim, D. W.; Tcho, I. W.; Kim, J. K.; Kim, M. S.; Choi, Y. K. Triboelectric nanogenerator: Structure, mechanism, and applications. *ACS Nano* **2021**, *15*, 258–287.

[45] Gao, Q.; Cheng, T. H.; Wang, Z. L. Triboelectric mechanical sensors—Progress and prospects. *Extreme Mech. Lett.* **2021**, *42*, 101100.